Available online at www.sciencedirect.com
ScienceDirect
Journal of Nuclear Materials 367–370 (2007) 1549–1556
journal of nuclear materials
www.elsevier.com/locate/jnucmat

The role of small specimen test technology in fusion materials development

G.E. Lucas [a,*], G.R. Odette [a], H. Matsui [b], A. Möslang [c], P. Spätig [d], J. Rensman [e], T. Yamamoto [a]

[a] Department of Mechanical and Environmental Engineering, UC Santa Barbara, Santa Barbara, CA 93106, USA
[b] International Research Center for Nuclear Materials, Institute for Materials Research, Tohoku University, Oarai, Ibaraki-ken 311-1313, Japan
[c] Forschungszentrum Karlsruhe, IMF-I, P.O. Box 3640, D-76201 Karlsruhe, Germany
[d] EPFL/CRPP, Fusion Technology Materials, OVGA/2, CH – 5232 Villigen PSI, Switzerland
[e] NRG, P.O. Box 25, 1755 ZG Petten, The Netherlands

Abstract

Small specimen test technology (SSTT) has long been an integral part of fusion materials development. Past work has led to an array of techniques that not only have provided a means of efficiently using available irradiation volumes but have also led to improving insights and understanding of the role of specimen size in deformation and fracture phenomena. As the fusion community increases its focus on design and construction of next generation fusion machines, the ability of SSTT to provide the requisite design data as well as insights to behavior beyond the evolving data base will be critical. This paper will provide a context of the past and present work on SSTT and explore the opportunities to build on past successes to address future needs.

1. Background

The development and application of small specimen test technology (SSTT) has proceeded in parallel with the development of materials for fusion reactors [1–3]. The driving force has largely been the need to use irradiation sources with constrained volumes and high heating rates. To date, this has mainly involved materials test reactors and accelerator-based irradiations, but the persistent expectation has been that a high energy neutron source – currently thought to be IFMIF – would ultimately provide the extrapolation of fission-reactor-based irradiation data to a fusion neutron environment, and thus serve to develop a design basis for the structural materials for a DEMO-type reactor.

Work to date has developed an array of techniques to extract mechanical properties – such as tensile data, fatigue, fracture toughness, impact properties, creep and fatigue crack growth – from relatively small specimens [1–3]. Corresponding specimens with major dimensions of the order

* Corresponding author. Tel.: +1 805 893 2126; fax: +1 805 893 7712.
E-mail address: gene.lucas@evc.ucsb.edu (G.E. Lucas).

0022-3115/$ - see front matter © 2007 Elsevier B.V. All rights reserved.
doi:10.1016/j.jnucmat.2007.04.034

25 mm are commonly used in fission reactor irradiations, and procedures for fabricating and testing these specimens have been largely derived from ASTM standards. Hence, test matrices for the IFMIF are being designed to first order with these specimens in mind [4].

A number of differences remain to be reconciled, however, before IFMIF matrices can be finalized. For instance, there are several tensile specimen geometries in use that differ slightly in size and geometry; and although the size and geometry-dependencies of the data are well known [1], a final decision for IFMIF applications has yet to be made. Similarly, the pros and cons of hourglass versus cylindrical geometry for fatigue specimens have been outlined, but there remain adherents of each approach. And the volume and constraint advantages of compact tension (CT) over bend geometries for fracture toughness testing must be weighed against the versatility of the bend geometry for impact and dynamic testing. In all cases, the fundamental knowledge base is sufficient to support an extended international program of round robin testing and optimization to converge on a set of specimen geometries. Optimizing the IFMIF test matrices themselves will require a more extended analysis to balance, for instance, the specimen type and redundancy, number of materials characterized, irradiation conditions, etc.; and this in turn will require a greater interaction between the materials and the design communities. It is clear that, in any case, there will be ample room in IFMIF irradiation matrices to include specimens to develop both a design data base for a small number of candidate structural materials, as well as to provide science-based experiments to better understand microstructure-property correlations and to justify moderate extrapolations beyond existing databases.

Indeed, SSTT has fostered a science-based approach to its own development, providing opportunities to explore and characterize deformation and fracture behavior beyond test techniques based on more conventional approaches. Moreover, it is clear that next generation machines will necessitate the development and application of specimens and techniques beyond those described above, with an increased focus on materials behavior not yet well characterized. Hence, the purpose of this paper is to provide an update on SSTT developments, particularly in the areas of deformation and fracture, and to explore some opportunities to build on past successes for future needs.

2. Fracture

Much of the recent work on fracture assessment has addressed the development and application of the master curves-shifts, MC-ΔT, method developed by Odette [5,6] as an extension of the approach first proposed by Wallin, that has evolved to an ASTM standard [7,8]. The MC-ΔT method has been applied to bcc alloys currently being considered as candidates for fusion reactor structures – namely, tempered ferritic/martensitic steels (FMS) and vanadium-based alloys. Based on empirical observations, the approach assumes that the shape of the effective fracture toughness K_e as a function of test temperature, T, is described by a universal MC, or small family of curves, $K_{mc}(T - T_0)$, which is indexed by a reference temperature T_0 at a reference toughness K_r. The curve is adjusted in temperature space to account for both intrinsic and extrinsic effects. For instance, curves can be adjusted to conditions of higher or lower constraint (e.g., larger or smaller specimen dimensions) associated with size and geometry [9]. Additional shifts can also be imposed to account for statistical weakest link-type size effects [10]. The position of the curve can also adjusted using additional shifts, ΔT, to account for strain rate, ΔT_{sr}, irradiation, ΔT_i, as well as a margin of safety, ΔT_m.

Several systematic studies have recently been undertaken at UCSB in conjunction with Petten and EPFL/CRPP to address size effects on $K_e(T)$ due to weakest link statistics and constraint effects. A statistical size adjustment (SA) scaling with $B^{1/4}$, where B is the fracture specimen thickness, can be derived from weakest link statistics per the ASTM E1921 procedure [10]. Moreover, a constraint loss adjustment (CLA) based both on B and fracture specimen ligament size, b, can be derived from combining finite element method (FEM) simulations of crack tip fields with critical stress–critical area, σ^*–A^*, micromechanics of cleavage fracture in bcc metals [8,9,11,12]. As an example, these size adjustment analyses have been recently applied to a toughness database generated on the 14 mm Eurofer97 plate in the T–S orientation. The specimen matrix is shown in Fig. 1(a), characterized by systematic variations in both B (1.5–9.8 mm) and b (1.7–7 mm). The measured toughness, K_{Jm} (eight specimens tested for each specimen type, with K_J derived from J), at −141 °C is shown in Fig. 1(b) plotted against B for various b. The data clearly show both statistical and constraint loss size effects. The size adjust-

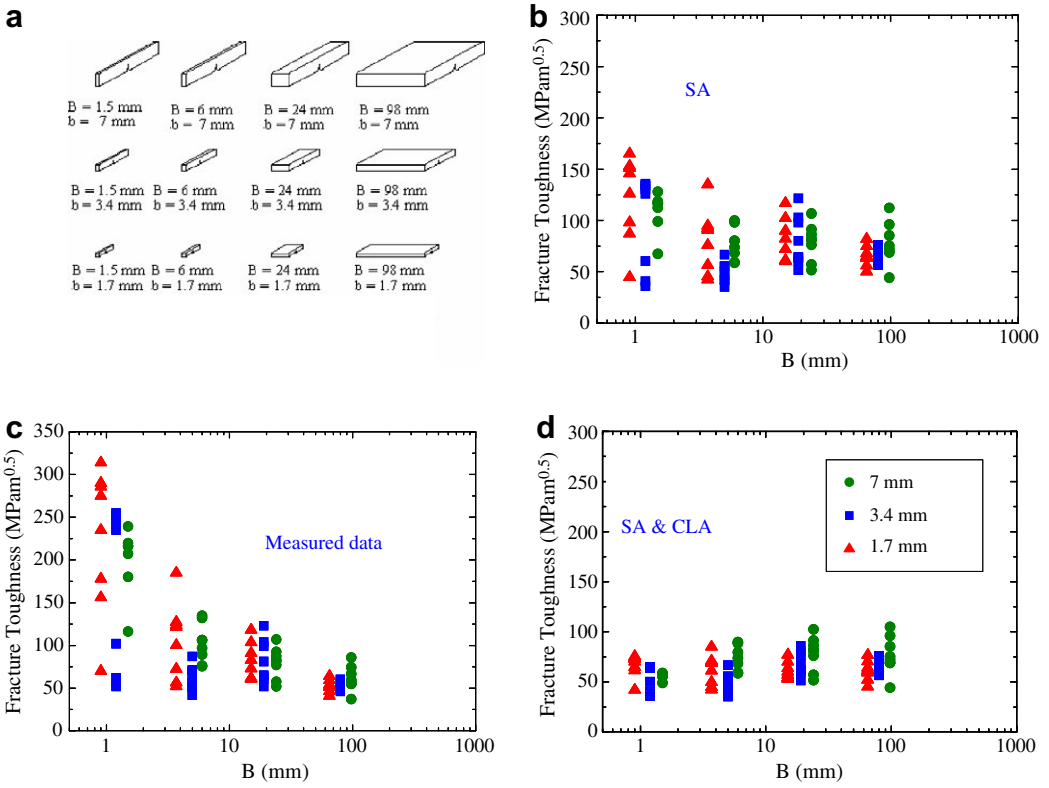

Fig. 1. Size effects experiment and analysis on the 14 mm plate of Eurofer97.

ments to the fracture toughness, K_{Jr}, are shown in Fig. 1(c) and (d). The variations in K_{Jr} in Fig. 1(c) shows the remaining effect of constraint loss after statistical size adjustment (SA). Fig. 1(d) shows that after both SA and CLA the K_{Jr} exhibit a much more self-consistent and homogeneous data population, although the smallest specimens may be somewhat over-adjusted. Overall, these results are broadly consistent with constraint loss effects found in a similar study on F82H [13].

Note the size adjustment procedure can be used to evaluate the stress and strain conditions leading to cleavage fracture in thin-walled fusion structures with shallow surface cracks, representing conditions of large constraint loss [14]. This is important since, coupled with statistical effects of a cracked body's size, the effective strength and ductility of such structures are higher compared to those for thick sections, such as pressure vessels. This means that the effects of irradiation embrittlement may be somewhat mitigated in the case of fusion structures.

Despite success to date, there remain a number of issues to be resolved with respect to the MC approach. These include, but are not limited to: (1) whether a single MC exists versus a family of curves for different alloys; (2) the fundamental basis for the master curve itself; (3) sampling statistics of small specimens for heterogeneous (and thus high inherent scatter) material; and (4) the effects of irradiation on loss of strain hardening, leading to increasingly rapid loss of constraint in small specimens [9].

With respect to irradiation-induced ΔT_0 shifts, it has been previously shown that below about 400 °C irradiation embrittlement ($\Delta T_i > 0$) is generally dominated by corresponding increases in a bcc alloy's yield strength, $\Delta\sigma_y$ [5,14–16]. As an example, Fig. 2 plots increases in the room temperature $\Delta\sigma_y$ versus ΔT_i for all available data on F82H for irradiations between irradiation temperatures of about $T_{ir} \approx 250$–385 °C and displacement doses between ≈0.04 and 5 dpa. The least square fit $\Delta T_i/\Delta\sigma_y = C_o \approx 0.58$ °C/MPa is consistent with previous estimates [14]. While this value is somewhat less than that observed for low dose irradiations of RPV steels – $C_o \approx 0.7$ °C/MPa – the difference can be readily explained by the corresponding difference between the strain hardening in the two cases [17].

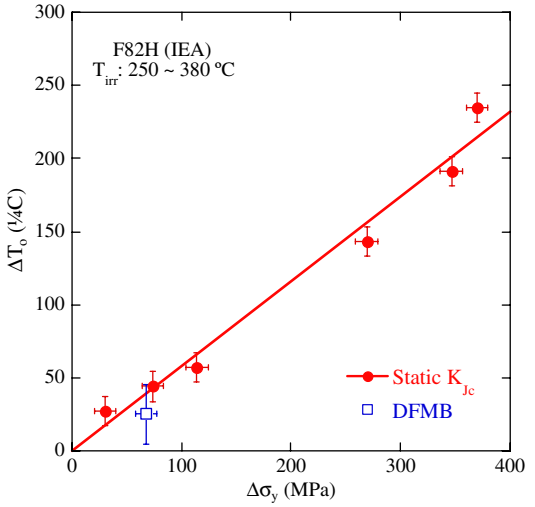

Fig. 2. Relation between $\Delta\sigma_y$ and ΔT_i (thus ΔT_0) for F82H in the hardening-dominated embrittlement regime.

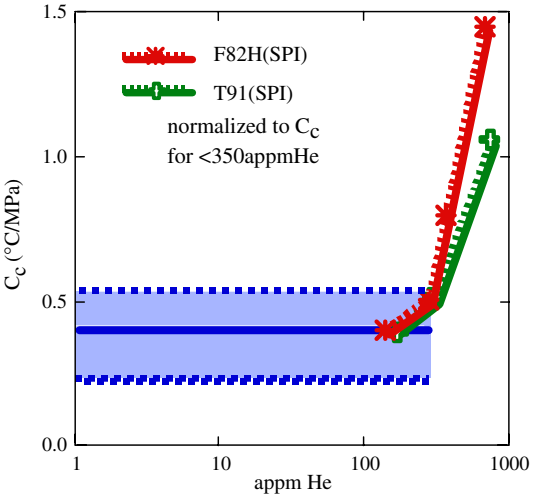

Fig. 3. Neutron and spallation proton irradiation estimated $C_c = \Delta T_c/\Delta\sigma_y$ showing a significant effect of helium above about 650 appm accompanied by a transition to intergranular fracture.

There is an ongoing debate on the effect of helium on hardening and embrittlement at lower $T_i \leqslant \approx 400$ °C. There is little indication that, at least up to levels of 1000 appm, helium has a significant effect on $\Delta\sigma_y$, except, perhaps at low irradiation temperatures [15]. However, there is accumulating evidence that synergistic interactions between high levels of helium, in excess of 500–600 appm, leading to grain boundary weakening, combined with large $\Delta\sigma_y$ for T_i below 400 °C, may result in very brittle intergranular fracture (IGF) and a corresponding enormous ΔT_i. A simple model for this hypothesis has been obtained at UCSB by using the very limited available literature data to estimate the effect of very high helium levels on C_c ($=\Delta T_c/\Delta\sigma_y$, where ΔT_c is the Charpy-based irradiation-induced shift) and, by analogy, C_o [15]. The shaded region in Fig. 3 shows the one standard deviation scatter band of C_c up to several hundred appm helium for a large number of tempered martensitic steels (TMS). The dashed lines are normalized estimates of C_c for spallation proton irradiations derived from small punch fracture tests reported by Dai et al. [18]. The highest points, with equivalent C_c between ≈1.1 and 1.5 °C/MPa, are for irradiations at $T_{ir} \approx 275$ °C and 680–770 appm helium. These high C_c values compare to an average value of 0.4 °C/MPa at lower helium. That is, at these high helium levels, an increment of $\Delta\sigma_y$ produces between about 2.5 and 4 time larger ΔT_c than for helium below about 500 appm. Most notably, the high values of C_c are accompanied by a transition from transgranular cleavage to IGF.

This behavior can be rationalized in terms of a gradual reduction in grain boundary fracture strength relative to that for intergranular cleavage associated with the accumulation of helium, ultimately resulting in an intergranular fracture path [14,15]. If verified, such large ΔT_i would effectively eliminate low activation martensitic steels as candidate alloys for post-ITER applications to fusion power demonstration reactors, at least for a range of lower service temperatures. Combinations of softening, creep, fatigue and irradiation induced damage (including swelling), and irradiation enhanced non-hardening embrittlement may set a relatively low upper limit on the service temperatures of TMS. Thus there is clear urgency to resolve the magnitude of this helium embrittlement effect in order to identify a viable materials system for the structure of a fusion demonstration reactor.

Work has also continued to progress on reducing the specimen size for ductile fracture testing. Work by Kasada and Kimura [19] and Kurishita et al. [20] have advanced the application of the unloading compliance approach to measuring ductile tearing toughness in subsized CT and bend bar geometries, respectively, down to 3.3 mm thicknesses.

Even smaller specimens, so-called deformation and fracture minibeams (DFMBs), with typical dimensions of $1.67 \times 1.67 \times 9.2\ \text{mm}^3$, have been developed at UCSB and are perhaps the smallest

pre-cracked specimens ever used to evaluate 'fracture toughness'. A large number of DFMBs have been included in the recent US-Japan HFIR program focusing on both vanadium alloys and reduced activation normalized TMS [21]. Due to massive constraint loss, and their corresponding very steep transition-toughness temperature curves, DFMBs are primarily intended to measure shifts in the cleavage transition temperature under (primarily) dynamic loading conditions (ΔT_d), but not necessarily fracture toughness or MC reference temperature shifts (ΔT_0) per se. Recently, irradiations in JMTR of the IEA program heat of F82H to 0.1 dpa at 290 °C have been carried out to demonstrate these small specimen test methods on irradiated material, as well as to add to the TMS irradiated property database [22]. The JMTR irradiations also included SSJ2-type sheet tensile specimens ($4 \times 16 \times 0.5\ mm^3$) at doses of 0.04 and 0.12 dpa. The post irradiation tests were carried out at the IMR-Oarai Center, Tohoku University. The results are shown in Fig. 4. The ΔT_d derived from dynamic DFMB tests was 25 ± 20 °C in reasonably good agreement with the estimated ΔT_i shifts described previously from tests on 1/3-sized pre-cracked Charpy bend bars, with dimensions of $3.3 \times 3.3 \times 18.3\ mm^3$, at a similar dose of 0.12 dpa, with a $\Delta T_0 \approx 43$ °C, after dose adjustment. As shown in Fig. 2, the corresponding $C_d = \Delta T_d/\Delta\sigma_y \approx 0.4$ °C/MPa is lower than the nominal $C_o \approx 0.58$ °C/MPa, but the difference is well within the expected data scatter.

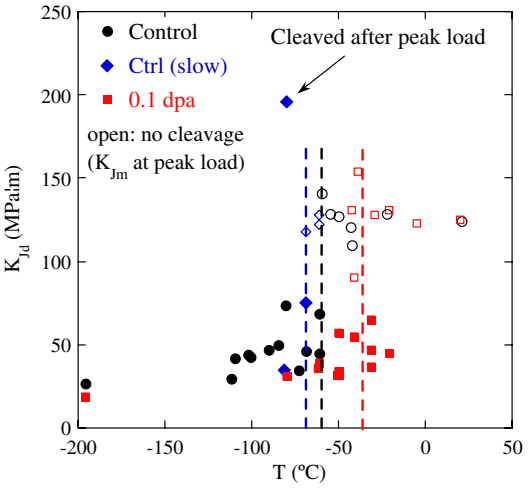

Fig. 4. Illustration of the irradiation-hardening shifts in transition temperature of F82H measured by DFMB specimens.

3. Fatigue

Efforts have continued both in Japan and Germany to reduce the size scale of fatigue specimens. Hirose et al., have developed small hourglass–shaped specimens which provide *S–N* (stress amplitude, *S*, versus number of cycles to failure, *N*) data similar to larger specimens [23]. The hourglass geometry offers the ability to achieve high strain ranges in push–pull fatigue tests, and some advantage in temperature control of the small gage section. Möslang [24] have developed a miniature fatigue specimen with a cylindrical gage section, approximately 2 mm in diameter and 7.6 mm in length. *S–N* results as well as cyclic stress–strain curves on these specimens are also in good agreement between data with much larger standard specimens. While the cylindrical geometry presents some testing challenges, it offers some advantages over the hourglass: the strain ranges of technological interest are more readily achievable and a greater volume and surface area can be tested for the same overall specimen size. The cylindrical geometry may also have some advantages in developing tests to address problems of thermo-mechanical and creep fatigue, discussed later. These are issues that remain to be resolved.

4. Deformation

Test techniques to characterize the constitutive behavior $\sigma(\varepsilon)$ of irradiated materials have continued to evolve, based on miniature tensile tests, various kinds of punch tests as well as microhardness and instrumented hardness tests [1,2]. Considerable advances have been obtained by linking these tests to FEM modeling of the deformation process. Two recent examples are shown here.

Spherical punch tests have been modeled by Spätig et al. [25] for sheet specimens clamped between an upper and lower die, using a relatively wide range of input constitutive equations. The effect of constitutive behavior on the punch load–displacement curve typically measured in a punch test showed that the post-yield part of the load–displacement curve is influenced by the strain hardening behavior, and this can influence the estimate of yield load and hence yield stress in the punch test. This work has also shown that the slope of the load–displacement curve in this region correlates well with an average flow stress in the strain region corresponding to the punch test. This is illustrated in

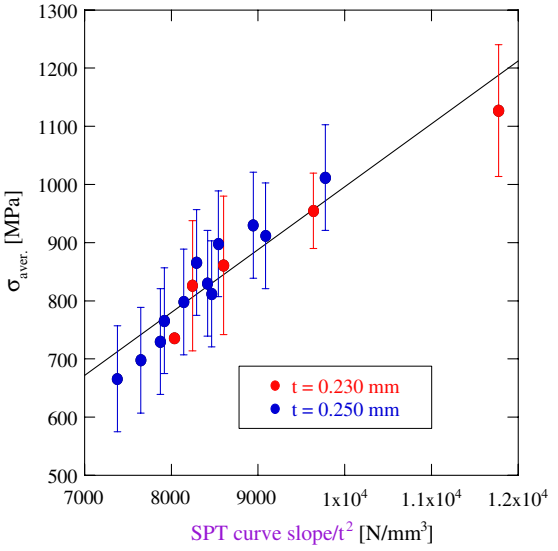

Fig. 5. Relationship between the slope of the small punch-displacement test and average flow stress derived from FEM simulations.

Fig. 5. The ability of the test to measure flow as well as yield stress may offer promise to characterizing constitutive behavior under multi-axial stress conditions.

Similarly, FEM simulations at UCSB of the hardness test have revealed a unique, universal relationship between the hardness, H, and the flow stress of the material averaged over a specified strain range [26]. A series of hardness FEM simulations were obtained using a constitutive relation $\sigma(\varepsilon)$ of the form

$$\sigma(\varepsilon) = \sigma_y \quad \varepsilon \leqslant \sigma_y, \tag{1a}$$

$$\sigma(\varepsilon) = \sigma_y + C[1 - \exp -\gamma(\varepsilon - \varepsilon_y)] \quad \varepsilon > \varepsilon_y, \tag{1b}$$

for a Luder's strain of $\varepsilon_y = 0.005$, and a wide range of σ_y (100–850 MPa), and maximum stain hardening levels ($C = 125$–500 MPa) and pre-saturation hardening rates ($\gamma = 3$–15). Values of elastic modulus were varied from $E = 50$–400 GPa. Corresponding simulations were carried out for a very large number of empirically derived $\sigma(\varepsilon)$ curves as well, so that direct comparisons could be made between the predictions and measurements.

The FEM H data for the various $\sigma(\varepsilon)$ were analyzed by calculating an average flow stress $\langle\sigma_{sh}\rangle$ between various lower (ε_l) and upper (ε_u) limits and fitting the corresponding $\sigma_{flow} = \sigma_y + \langle\sigma_{sh}\rangle$ versus H data. A very good fit for the strain range is 0–10%, as shown by the solid line in Fig. 6, is given by

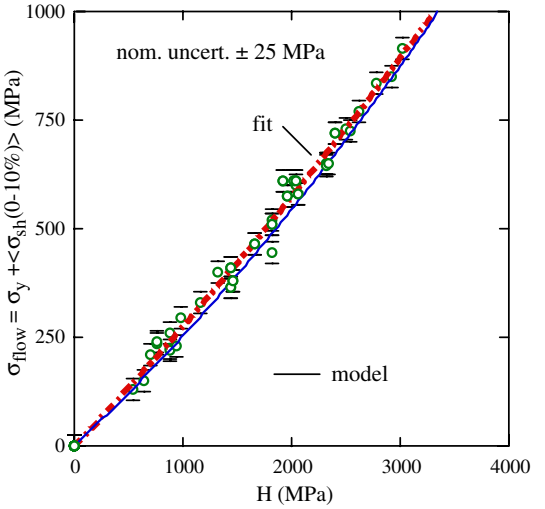

Fig. 6. The value of $\sigma_{flow} = \sigma_y + \langle\sigma_{sh}\rangle$ versus H for a wide range of $\sigma(\varepsilon)$ derived from FEM simulations of the hardness test.

$$H = 4.05(1 - 34.6\sigma_{flow}/E)\sigma_{flow}. \tag{2}$$

The symbols are σ_{flow}–H data pairs measured for a large number of materials, again covering a large range of $\sigma(\varepsilon)$. The agreement is very good, although a fit to the data shown by the dashed line has a slightly different shape than the predicted curve.

The universal master σ_{flow}–H relation is remarkable in view of the much larger ε-range created by the indentation than in tensile tests. It provides a quantitative understanding of a number of empirical trends; for instance: (1) that there is a large variation in the observed H/σ_y ratios due to the effects of both $\langle\sigma_{sh}\rangle$ and σ_{flow}/E; (2) that the ratio of H/σ_y tends to be higher for steels with low σ_y due to the effect of σ_{flow}/E; and (3) that the $\Delta H/\Delta\sigma_y$ following irradiation is generally lower than the unirradiated H/σ_y due to reductions in $\langle\sigma_{sh}\rangle$. In addition, the universal relation allows combining H and σ_y measurements from a tensile test to estimate strain hardening in alloys with very low uniform tensile strain as

$$\langle\sigma_{sh}\rangle = \sigma_{flow}(\text{from } H) - \sigma_y \text{ (from a tensile test)}. \tag{3}$$

The universal relation also permits a convenient method to evaluate $\sigma(\varepsilon)$ in high ε regions by making H measurements on pre-strained materials. For instance, an effective way to do this is to make hardness transverses on sections of a bent beam that undergoes stable plastic deformation over a wide range of effective ε. Indeed, such transverses from regions of high deformation across the neutral axis

not only assess regions with ≈0 to very high ε, but also involve complex and varying stress state that yield information on plasticity flow laws and tensile-to-compressive deformation effects on σ(ε).

These recent illustrations of combining FEM simulations with SSTT illustrate the power of combining modeling and experiment to both understand underlying deformation behavior and to extend the applicability of the techniques to obtaining both fundamentally and practically useful information.

5. Conclusions

SSTT has reached a significant level of maturity. A number of specimens and techniques are now routinely used in reactor irradiation experiments to obtain a range of important mechanical properties. To first order, these specimens and techniques are available to IFMIF irradiations. However, resolving the minor differences among laboratory specimen geometries and procedures may require an international effort of focused round robin testing and selection. Balancing and refining the IFMIF irradiation matrices also remain as major objectives.

Although a number of techniques are available and applicable to IFMIF irradiations, a number of properties must be assessed for future machines for which there is yet well developed SSTT. This is particularly true for DEMO design and beyond. These include the various forms of fatigue failure beyond simple *S–N* data; for instance fatigue crack growth, low cycle fatigue, thermo-mechanical fatigue, and creep–fatigue are all important phenomena which require characterization; while some of the specimens and techniques developed to date may be applicable to obtaining these data, demonstration and a significant data base await further development. Moreover, stress relaxation – particularly radiation enhanced/induced stress relaxation – will be an important design consideration; and while stress relaxation behavior can be derived from creep data for which there is a well developed SSTT, this may not sufficiently account for phenomena such as transient creep; and hence appropriate testing and analysis must develop to address this. As a final example, high temperature constitutive behavior will be an important input to the structural analysis codes for component design. While tensile tests based on SSTT can be one source of data, it will be important to derive flow properties from other specimen geometries to interrogate, for instance, the effects of stress state. Helium effects will be an important consideration here, and many of the various techniques to generate helium in irradiated material will require the implementation of the small volumes associated with SSTT.

Hence, SSTT will continue to be a critical part of materials development for fusion reactors. As illustrated here, with a few examples, there exists a wealth of opportunities to integrate SSTT with modeling (as well as non-destructive testing, microstructural and microchemical analyses) to greatly extend the understanding and application of flow and fracture information derived from these tests.

References

[1] G.E. Lucas, G.R. Odette, M. Sokolov, P. Spatig, T. Yamamoto, P. Jung, J. Nucl. Mater. 307–311 (2002) 1600.
[2] P. Jung, A. Hishinuma, G.E. Lucas, H. Ullmaier, J. Nucl. Mater. 232 (1996) 186.
[3] G.E. Lucas, J. Nucl. Mater. 117 (1983) 327.
[4] M. Seki, J. Nucl. Mater., these Proceedings.
[5] G.R. Odette, K. Edsinger, G.E. Lucas, E. Donahue, in: Small Specimen Test Techniques, ASTM STP 1329, vol. 3, American Society for Testing and Materials, 1998, p. 298.
[6] G.R. Odette, G.E. Lucas, J. Nucl. Mater. 283–287 (2000) 518.
[7] K. Wallin, in: M. Kirk, A. Bakker (Eds.), Constraint Effects in Fracture: Theory and Applications, ASTM STP 1244, ASTM (1994), p. 519.
[8] ASTM E 1921-03, in: Annual Book of ASTM Standards, American Society for Testing and Materials, 2003.
[9] G.R. Odette, M.Y. He, J. Nucl. Mater. 353 (2002) 1624.
[10] H.J. Rathbun, G.R. Odette, T. Yamamoto, G.E. Lucas, Eng. Fract. Mech. 73 (2006) 134.
[11] H.J. Rathbun, G.R. Odette, M.Y. He, T. Yamamoto, Eng. Fract. Mech., in press.
[12] G.R. Odette, M.Y. He, J. Nucl. Mater. 283–287 (2000) 120.
[13] G.R. Odette, T. Yamamoto, H. Kishimoto, M. Sokolov, P. Spatig, W.J. Rensman, G.E. Lucas, J. Nucl. Mater. 329–333 (2004) 1243.
[14] G.R. Odette, T. Yamamoto, H.J. Rathbun, M.Y. He, M.L. Hribernik, J.W. Rensman, J. Nucl. Mater. 323 (2003) 313.
[15] T. Yamamoto, G.R. Odette, H. Kishimoto, J.-W. Rensman, P. Miao, J. Nucl. Mater., in press.
[16] S. Jitsukawa, A. Kimura, A. Kohyama, R.L. Klueh, A.A. Tavassoli, B. van der Schaaf, G.R. Odette, J.W. Rensman, M. Victoria, C. Peterson, J. Nucl. Mater. 329–333 (2004) 39.
[17] M.Y. He, G.R. Odette, T. Yamamoto, J. Nucl. Mater., these Proceedings.
[18] Y. Dai et al., private communication.
[19] R. Kasada, A. Kimura, J. Nucl. Mater., these Proceedings.
[20] H. Kurishita, T. Yamamoto, T. Nagasaka, A. Nishimura, T. Muroga, S. Jitsukawa, Mater. Trans. 45 (2004) 936.
[21] R.E. Stoller, H. Tanigawa, Planning of the US-JAPAN JP-26 Experiment for Irradiation in the HFIR, Fusion Materials Semiannual Report 1/1 to 6/30/2003 DOE/ER-313/34 (2003), p. 147.
[22] T. Yamamoto, G.R. Odette, D. Gragg, H. Kurishita, H. Matsui, W.J. Yang, M. Narui, M. Yamazaki, J. Nucl.

Mater., these Proceedings, doi:10.1016/j.jnucmat.2007.03.046.
[23] T. Hirose, H. Sakasegawa, A. Kohyama, Y. Katoh, H. Tanigawa, in: ASTM STP 1405, Americ Society for Testing and Materiasl, Conshohoken, PA, 2001, p. 535.
[24] A. Möslang, private communication.
[25] P. Spätig et al., J. Nucl. Mater., these Proceedings, doi:10.1016/j.jnucmat.2007.03.038.
[26] M.Y He, G.R. Odette, T. Yamamoto, D. Klingensmith, J. Nucl. Mater., these Proceedings, doi:10.1016/j.jnucmat.2007.03.044.